Can We Detect Urban-Scale CO_2 Emission Changes Within Medium-Sized Cities?

Derek V. Mallia[1] , Logan E. Mitchell[1,2] , Andres Eduardo Gonzalez Vidal[1], Dien Wu[3], Lewis Kunik[1], and John C. Lin[1]

[1]Department of Atmospheric Sciences, University of Utah, Salt Lake City, UT, USA, [2]Utah Clean Energy, Salt Lake City, UT, USA, [3]Division of Geological and Planetary Sciences, California Institute of Technology, Pasadena, CA, USA

Abstract The COVID-19 pandemic resulted in a widespread lockdown during the spring of 2020. Measurements collected on a light rail system in the Salt Lake Valley (SLV), combined with observations from the Utah Urban Carbon Dioxide Network observed a notable decrease in urban CO_2 concentrations during the spring of 2020 relative to previous years. These decreases coincided with a ~30% reduction in average traffic volume. CO_2 measurements across the SLV were used within a Bayesian inverse model to spatially allocate anthropogenic emission reductions for the first COVID-19 lockdown. The inverse model was first used to constrain anthropogenic emissions for the previous year (2019) to provide the best possible estimate of emissions for 2020, before accounting for emission reductions observed during the COVID-19 lockdown. The posterior emissions for 2019 were then used as the prior emission estimate for the 2020 COVID-19 lockdown analysis. Results from the inverse analysis suggest that the SLV observed a 20% decrease in afternoon CO_2 emissions from March to April 2020 (-90.5 tC hr^{-1}). The largest reductions in CO_2 emissions were centered over the northern part of the valley (downtown Salt Lake City), near major roadways, and potentially at industrial point sources. These results demonstrate that CO_2 monitoring networks can track reductions in CO_2 emissions even in medium-sized cities like Salt Lake City.

Plain Language Summary High-density measurements of CO_2 were combined with a statistical model to estimate emission reductions across Salt Lake City during the COVID-19 lockdown. Reduced traffic throughout the COVID-19 lockdown was likely the primary driver behind lower CO_2 emissions in Salt Lake City. There was also evidence that industrial-based emission sources may of had an observable decrease in CO_2 emissions during the lockdown. Finally, this analysis suggests that high-density CO_2 monitoring networks could be used to track progress toward decarbonization in the future.

1. Introduction

With the effects of climate change expected to intensify through the 21st century, urgent action is needed to reduce humanity's dependence on fossil fuels (IPCC, 2018). Carbon dioxide (CO_2) is a greenhouse gas (GHG) emitted from the combustion of fossil fuels and is the main driver behind rising global temperatures (IPCC, 2013). Given that half of anthropogenic CO_2 is emitted from urban areas (Roest et al., 2020), cities will play a pivotal role towards decarbonization efforts. Therefore, quantifying CO_2 emissions at the city-scale will be important for determining whether cities are meeting CO_2 decarbonization targets (Ciais et al., 2014; Gurney et al., 2015; Hsu et al., 2019).

Quantifying CO_2 emissions is an inherently difficult task since directly measuring emissions at the urban scale is challenging. Therefore, bottom-up approaches like emission inventories are often used to estimate CO_2 emissions. Emission inventories are constructed using well-established protocols and standards that combine activity data and emission factors across a variety of scales (Gurney et al., 2020, 2021). While emission uncertainties at the national scale are relatively low (<10%), these uncertainties are far greater at regional (~20%) and local scales (50%–250%) and are most pronounced in urban areas (Gately & Hutyra, 2017). For cities where CO_2 measurements are available, CO_2 concentrations can be used to back-calculate emissions. This method is referred to as a "top-down" modeling approach. Observations can also help constrain existing emission inventories through inverse models. Inverse modeling approaches are often referred to as a "hybrid" method where observations adjust a first guess emission estimate, usually provided by an emission inventory (Nisbet & Weiss, 2010). Hybrid modeling approaches have been widely used to constrain emissions for cities across the globe, including Paris (Breon

Software: Derek V. Mallia, Lewis Kunik, John C. Lin
Supervision: Derek V. Mallia, John C. Lin
Validation: Logan E. Mitchell
Visualization: Derek V. Mallia, Logan E. Mitchell, Andres Eduardo Gonzalez Vidal
Writing – original draft: Derek V. Mallia
Writing – review & editing: Derek V. Mallia, Logan E. Mitchell, Andres Eduardo Gonzalez Vidal, Dien Wu, Lewis Kunik, John C. Lin

et al., 2015; Staufer et al., 2016), Indianapolis (Lauvaux et al., 2016; Oda et al., 2017), Cape Town (Nickless et al., 2018), the San Francisco Bay Area (Turner et al., 2020), New York City (Pitt et al., 2022), Washington DC/Baltimore (Yadav et al., 2021), Los Angeles (Yadav et al., 2021), and Salt Lake City (SLC; Mallia et al., 2020). These studies used a variety of CO_2 sampling strategies including ground-based CO_2 monitoring sites (Nickless et al., 2018; Turner et al., 2020; Yadav et al., 2021), tall towers (Breon et al., 2015; Lauvaux et al., 2016; Staufer et al., 2016), aircraft measurements (Pitt et al., 2022), ground-based mobile measurements (Mallia et al., 2020), and satellite observations (Oda et al., 2017).

While inverse models have been used to constrain emission estimates for cities, until recently, there has been limited work determining whether top-down and hybrid modeling approaches can detect rapid changes in CO_2 emissions. During the spring of 2020, governments around the world utilized non-pharmaceutical intervention strategies such as "lockdowns" to slow the spread of the coronavirus disease 2019 (COVID-19). These lockdowns dramatically reduced travel and resulted in more people working from home. Traffic reductions during the height of the lockdown varied from 30% to 75% depending on the city and region (Gensheimer et al., 2021). On a global scale, the COVID-19 lockdowns in 2020 resulted in annual CO_2 emission reductions of 7% relative to 2019 (Le Quéré et al., 2021). The COVID-19 lockdown provided a unique opportunity to determine whether hybrid modeling approaches could identify changes in urban CO_2 emissions at the city-scale based on observed differences in CO_2 during the lockdown period. On average, major metropolitan areas observed emission reductions during the COVID-19 lockdown that ranged between 30% and 55% (Lian et al., 2022; Nalini et al., 2022; Turner et al., 2020; Yadav et al., 2021) depending on the city. Reductions in traffic were thought to be the primary driver in emission reductions in Paris and the San Francisco Bay Area during the COVID-19 lockdown (Lian et al., 2022; Turner et al., 2020). It is also suspected that disruptions in the industrial/manufacturing sector may have also contributed to non-negligible emission reductions in Los Angeles. However, quantifying emission changes in these sectors is challenging without reliable activity data (Yadav et al., 2021). Given uncertainties surrounding atmospheric transport, instrument uncertainties, and background estimates of CO_2, it was suggested that top-down modeling approaches are limited to detecting emission reductions greater than 20% for urban areas (Lian et al., 2022). Network density was also highlighted as a factor that may limit urban-scale mapping of emission adjustments (Nalini et al., 2022). However, alternative observation techniques such as mobile-based measurement platforms have been shown to provide more detailed emission adjustments that can resolve city-scale emission patterns (Mallia et al., 2020).

In this study, we quantify the impacts of the COVID-19 lockdown on emissions across the Salt Lake Valley (SLV). The SLV is situated in northern Utah and is bounded by two large mountain ranges on the east and west sides, while the Great Salt Lake is located to the northwest (Figure 1). Downtown SLC is anchored to the northeastern part of the valley while the rest of SLC and its suburbs encompass the remaining part of the valley. Unlike other cities used to investigate emission reductions during the COVID-19 lockdown, the SLV is a medium-sized metropolitan area with a population of just over 1 million people and emits an order of magnitude less of CO_2 relative to larger cities like Los Angeles, San Francisco, and Washington DC/Baltimore (Gurney et al., 2020). Therefore, determining whether CO_2 emissions reductions are traceable for smaller cities and metropolitan areas is still an outstanding question. It is also worth noting that COVID-19 lockdown measures in SLC were less stringent relative to other cities across the U.S (Hallas et al., 2021), which suggests that emission reductions would be more difficult to detect. The SLV is home to two CO_2 networks. The first network includes in situ measurements collected at 5 sites located across the SLV, and a background site situated on the top of an adjacent mountain (Lin et al., 2018). The second network consists of a CO_2 instrument mounted on top of a light-rail train (aka "TRAX") that traverses the SLV (Mitchell, Crosman, et al., 2018).

Here, we used a Bayesian Inverse model to constrain emissions for the SLV for a non-COVID-19 time period (spring 2019) and during the first COVID-19 lockdown (spring 2020). This framework was used to quantify valley wide emission reductions and to identify areas and sectors where CO_2 emission reductions were the greatest. The Methodology (Section 2) describes the inverse model configuration, the measurements used in this analysis, and other model inputs such as emissions and emission uncertainties. Section 3 analyzes the inverse model results. The summary section (Section 4) highlights major findings from this study and identifies areas for future work.

2. Methodology

This section describes the methodology used to quantify the impacts of the COVID-19 lockdown on CO_2 emissions across the SLV. First, the mathematical framework used to constrain emissions across the SLV, that is, a Bayesian inverse model, is introduced in Section 2.1. This is followed up by Sections 2.2–2.5, which describes
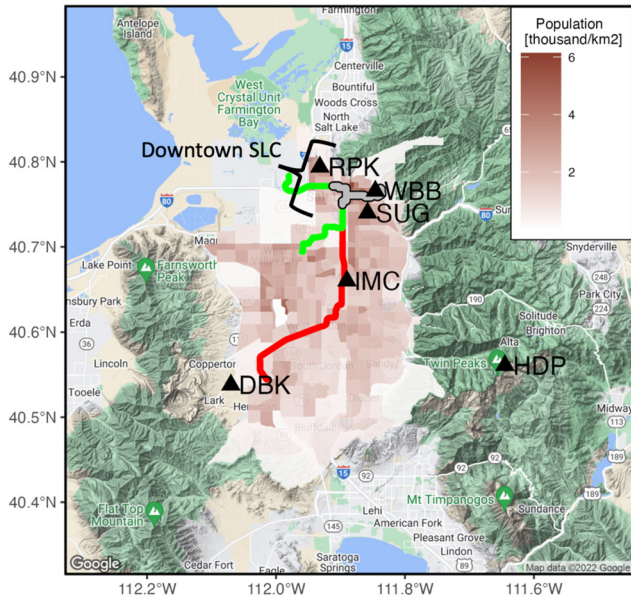
Figure 1. A map showing the Salt Lake Valley, the population density (brown shading), non-mobile CO_2 measurements sites (black triangles), and the TRAX Red and Green lines (green and red lines). The gray shaded line represents sections of the Red and Green lines that run through downtown SLC.

the various inputs needed to run the inverse model analysis such as anthropogenic emissions, biospheric fluxes, the atmospheric transport model, and CO_2 observations. Section 2.6 describes the general inverse model setup and configuration, while also providing details on how different model inputs were synthesized together to generate an inverse analysis for 2019 and then 2020.

2.1. Bayesian Inverse Model

Bayesian inverse models are commonly used tools to provide a top-down estimate of anthropogenic emissions of CO_2 by synthesizing prior information such as an emission inventory and observed concentrations of CO_2. An optimized estimate of anthropogenic emissions of CO_2, which will be referred to as the posterior emissions ($\hat{s}$), can be obtained by solving a cost function that incorporates sources of uncertainty and deviations between atmospheric observations and a prior emission inventory (Enting, 2002; Tarantola, 1987):

$$\hat{s} = s_p + (HQ)^T(HQH^T + R)^{-1}(z - Hs_p)$$

The prior or "first-guess" emission estimate (s_p) is defined here as a state vector with length of m, equal to the number of grid cells multiplied by the number of timesteps. The prior emission inventory used for the inverse analysis is discussed further in Sections 2.3 and 2.6. The Jacobian matrix (H) describes the spatiotemporal influence of each grid cell in our study domain for each observed CO_2 enhancement (z). H has dimensions of $n \times m$, where n is the number of observations, and is estimated using atmospheric footprints generated from atmospheric transport model simulations (see Section 2.3). For this study, z was defined as the observed enhancement of CO_2 due to anthropogenic emissions within the SLV and has dimensions of n. The observations used to estimate z are reviewed in Section 2.2, while Section 2.6 describes how the enhancement is calculated from the CO_2 observations. The prior covariance matrix (Q) has dimensions of $m \times m$ and describes the prior emission uncertainty and the spatiotemporal correlation of these uncertainties. More details behind the computation of Q can be found in the Supporting Information S1 (Text S1). The final variable in the cost function is the model-data mismatch matrix (R), which defines model-data uncertainties related to atmospheric transport and observed measurements, including contributions from biospheric and background CO_2. The R matrix has dimensions of $n \times n$. More details behind the definition of R, the different error terms, and the estimate of these terms are provided in the Supporting Information S1 (Text S2).

In summary, the objective of the Bayesian inverse model utilized here is to adjust the prior emissions inventory s_p based on deviations between observed (z) and model-predicted CO_2 enhancements (Hs_p) as defined by the term ($z - Hs_p$). The remaining term on the right-hand side $(HQ)^T(HQH^T + R)^{-1}$ determines how much the prior should be adjusted for any given grid cell within s_p based on prior emission uncertainties and errors prescribed by the model-data mismatch matrix. For example, if emission uncertainties are large and errors prescribed by R are small, this gives the inverse model more flexibility to adjust the prior emissions s_p based on deviations between the observations and model-predicted concentrations of CO_2. The ability for the inversion to adjust the prior emission estimate will be limited if the model-data mismatches are large, the emissions have low uncertainty, and/or the deviations between the observed and modeled CO_2 concentrations are small.

2.2. Observations

Measurements from the Utah Urban Carbon Dioxide Network (UUCON) and a CO_2 instrument installed on a light-rail train car (TRAX) were used to estimate CO_2 concentrations across the SLV (Figure 1). The UUCON network, which is located within the SLV, is one of the world's longest running urban CO_2 networks (Lin et al., 2018). The UUCON network consist of 5 active stations that sample a variety of urban typologies (Figure 1). A sixth site, which is designated as Hidden Peak (HDP), is situated near the top of a nearby mountain with an elevation of 3,351-mASL and is ~20-km to the southeast of the SLV. The UUCON sites are instrumented with high-precision,

LiCOR 6262 or Los Gatos Research (LGR) ultraportable GHG instruments, which are calibrated with reference tanks traceable to the World Meteorological Organization's calibration scales (Bares et al., 2019; Mitchell, Lin, et al., 2018; Pataki et al., 2003).

A TRAX light-rail train car was outfitted with an LGR ultraportable GHG analyzer, which transects the SLV semi-continuously between 05:00 to 23:00 LST (Figure 1). The instrumented train car cycles between the TRAX Red and Green lines every 2–3 days. The Red and Green light rail trains take approximately 61 and 47 min to traverse their respective routes. Measurements of CO_2 from TRAX have a sampling frequency of 1 s, which were resampled to equally spaced points (∼35-m) along each of the transect lines (Mitchell, Crosman, et al., 2018). Explicit details behind the TRAX instrumentation setup, data calibration, and quality control assurance/control are described in Mitchell, Crosman, et al. (2018). Measurements along the TRAX line were averaged into 2-km segments, following recommendations by Mallia et al. (2020), which found that TRAX observations within 2-km bins were correlated with each other. For the TRAX Red and Green lines, this binning procedure resulted in 32 locations where CO_2 measurements are collected in the SLV.

The HDP site was used to estimate background concentrations of CO_2 for the SLV (Fasoli et al., 2018; Mallia et al., 2020; McKain et al., 2012; Mitchell, Lin, et al., 2018). The HDP site was established by the National Center of Atmospheric Research (Stephens et al., 2011) and maintenance of the site was taken over by the University of Utah and the UUCON network during the fall of 2016 (Bares et al., 2019). For this analysis, a 2-day running mean was used to smooth diurnal variability of CO_2 at HDP. Smoothed HDP data was used to represent background concentrations of CO_2.

2.3. Atmospheric Modeling

Backward trajectories from the Stochastic Time Inverted Lagrangian Transport model (STILT; Lin et al., 2003), which was recently merged with HYSPLIT (HYSPLIT-STILT; Loughner et al., 2021), were used to estimate the atmospheric footprint for each CO_2 measurement. The latest version of HYSPLIT v5.0.0 takes advantage of STILT's vertical turbulence scheme, which limits well-mixed backward trajectories from accumulating in regions with low turbulence. This version includes other STILT features such as treating boundary layer turbulence as a stochastic process (Lin et al., 2003). Lagrangian Particle Dispersion models like HYSPLIT-STILT have been widely used to carry out urban-scale inverse analyses (Kunik et al., 2019; Mallia et al., 2020; Pitt et al., 2022; Turner et al., 2020). The atmospheric footprint can be used to measure the sensitivity of concentration changes at a given location to upwind surface fluxes. The footprint (f) can be defined through the following:

$$f\left(x_r, t_r \mid x_i, y_j, t_m\right) = \frac{m_{air}}{h\overline{\rho}(x_i, y_j, t_m)} \frac{1}{N_{tot}} \sum_{p=1}^{N_{tot}} \Delta t_{p,i,j,k}$$

where m_{air} is defined as the molar mass of air (28.97 g mol^{-1}), and $\overline{\rho}$ is average density of HYSPLIT-STILT trajectories below height h. N_{tot} is the total number of backward trajectories within the trajectory ensemble, while $\Delta t_{p,i,j,k}$ is the total time that trajectories spend below the boundary layer height (h) at location x_i, y_j, t_m. An ensemble of 1,000 backward trajectories were used to construct the footprint for each receptor defined in this study. An ensemble number of 1,000 trajectories has been shown to limit run-to-run variability in trajectory model simulations (Mallia et al., 2015). Atmospheric footprints from HYSPLIT-STILT were output on a grid with $0.01 \times 0.01°$ spacing and used to construct the spatiotemporal influence matrix (H) for each observation. HYSPLIT-STILT footprints were convolved with emission fluxes to estimate CO_2 enhancements at each receptor.

Mass-coupled velocity fields from the Weather Research and Forecast model v4.2 (WRF; Skamarock et al., 2019) were used to drive HYSPLIT-STILT backward trajectories. Utilizing mass-coupled velocity fields instead of instantaneous winds from WRF improves mass conservation within HYSPLIT-STILT (Nehrkorn et al., 2010). WRF simulations were generated for March and April of 2019 and 2020 using a similar configuration described in Mallia et al. (2017, 2020). A detailed explanation behind the WRF model configuration can be found in the Supporting Information S1 (Text S3), while the WRF options selected can be viewed in Table S1 in Supporting Information S1.

2.4. Prior Emissions

A scaled version of the Vulcan 2010–2015 Version 3 emissions inventory (Gurney et al., 2020) was used as the prior emissions for the SLV. The Vulcan emissions inventory includes fossil fuel estimates of CO_2 for sectors including: onroad, offroad, airport, electricity production, industrial, commercial, residential, and cement.

Emissions from Vulcan are provided on a 1-km grid for 2015 at a temporal frequency of 1-hr. For this study, Vulcan emissions were subset to cover northern Utah and regridded to a $0.01 \times 0.01°$ grid. Since this study focuses on emissions for 2019 and 2020, emissions from Vulcan were scaled from 2015 to 2019. Emission changes from the Open-Data Inventory for Anthropogenic Carbon dioxide emission inventory (ODIAC; Oda et al., 2018), which covers 2000–2019, were used to scale Vulcan from 2015 to 2019. According to ODIAC, emissions slightly decreased across the SLV between 2015 and 2019 (-1.8%). Therefore, 2015 Vulcan emissions were scaled downwards by 1.8% for northern Utah. All grid cells within Vulcan for the SLV were scaled equally by -1.8%. The posterior emissions generated as part of the 2019 inverse analysis were used as the prior emissions for 2020. More details behind the rationale on using the 2019 posterior as prior for 2020 are discussed in Section 2.6. The spatiotemporal length scales, which were used to construct the prior covariance matrix, were set as 2 days and 6-km, respectively. The spatiotemporal length scale values selected here were based on a variogram analysis carried out by Kunik et al. (2019) and Mallia et al. (2020) for SLC.

2.5. Biospheric Fluxes

Biospheric fluxes for northern Utah for 2019 and 2020 were obtained from the Solar- Induced Fluorescence (SIF) for Modeling Urban biogenic Fluxes product (SMUrF version 1; Wu et al., 2021). SMUrF estimates gross primary production using SIF and combines this information with predictive variables to estimate plant respiration. Biospheric fluxes from SMUrF are natively gridded on a 5-km mesh that spans across Utah and is available from 2015 through July of 2020. Like the anthropogenic emissions, biospheric fluxes from SMUrF were regridded to a $0.01 \times 0.01°$ mesh to match the gridding of the HYSPLIT-STILT footprints.

2.6. Study Design

The first step of this analysis was to generate a prior emission estimate for the COVID-19 lockdown that more accurately reflects emissions observed across the SLV. Given the large uncertainties surrounding emission inventories at the local and regional scales (Gately & Hutyra, 2017), the first objective of this study was to optimize Vulcan emissions for a non-COVID-19 year by removing inherent emission errors. Posterior emissions from the 2019 inversion were then used as the prior emissions for the COVID-19 lockdown analysis. Through this design, any corrections made to the emissions would reflect emission changes solely due to the COVID-19 lockdown, and not necessarily changes related to prior emission uncertainties. Therefore, a Bayesian inverse analysis was first carried out for 2019, and then for 2020. For the Bayesian inverse analysis, this study only considered afternoon CO_2 observations (12:00–18:00 LST), which corresponds to a time when the planetary boundary layer is fully developed and modeled atmospheric transport errors are less pronounced (Breon et al., 2015; Gerbig et al., 2008; Lauvaux et al., 2016; Mallia et al., 2020; Yadav et al., 2021).

All measurements from the UUCON and TRAX networks were averaged to 6-hourly time bins before being incorporated within the inverse analysis for 2019 and 2020. For the 2019 analysis, all data from March and April were included. The 2020 analysis only included observations from March 15th through the end of April, which coincided with the peak of the COVID-19 lockdown. For the 2019 analysis, all observations in March were used instead of limiting the data to the last two weeks of the month since the primary objective of the 2019 inverse analysis was to create a more accurate emission estimate that could be used as a prior for the 2020 COVID-19 lockdown analysis. Emission corrections were applied to a domain bounded by -112.15 and $-111.73°$ longitude, and 40.4 and 41° latitude. Modeled biospheric flux contributions were included as part of the background and were removed from the observed CO_2 enhancement signal (z). Therefore, corrections were only applied to anthropogenic sources of CO_2 within the study domain following the methodology described in Mallia et al. (2020).

3. Results

3.1. Inverse Model Results 2019

For March–April 2019, seven UUCON sites were online and collecting CO_2 measurements (including HDP). During this time, the TRAX Red (Green) line made 117 (78) transects collecting CO_2 across the SLV during the afternoon hours (1800-0000 UTC).

The SLV exhibited significant spatiotemporal gradients in CO_2 during March and April of 2019 according to the TRAX measurements (Figure 2a). The highest CO_2 enhancements above background (dCO_2) were observed in
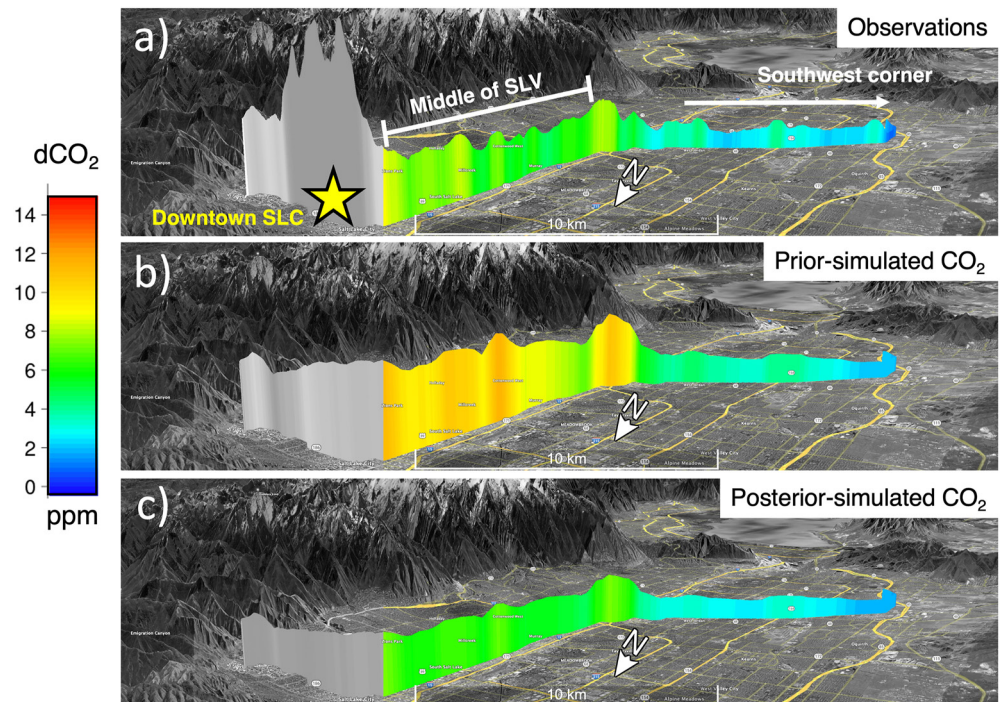
Figure 2. Afternoon-averaged dCO_2 along the TRAX Red line for March through April 2019. (a) Observed and model-simulated dCO_2 using the (b) prior and (c) posterior emissions. The color and height of the colored lines is proportional to the magnitude of dCO_2. The gray shaded lines for dCO_2 correspond to downtown SLC. dCO_2 concentrations in downtown SLC were not included as part of the inverse analysis.

downtown SLC, with values ranging between 10 and 25 ppm. As the TRAX Red line turns to the south, dCO_2 decreased by ~15 ppm and plateaued throughout the middle of the SLV with dCO_2 values ranging between 4 and 10 ppm. As the TRAX Red line veered to the southwest corner of the SLV, dCO_2 concentrations decreased again by 4 ppm. The northern part of the SLV is primarily dominated by emissions from traffic, electricity generation from 4 local power plants, industrial sources, and commercial activity (Figure 3) and has the highest emission rates (Figure 4a). The middle of the SLV is primarily composed of major roadways such as I-15, I-215, and I-80, along with other heavily trafficked non-highway roads. This region also has some commercial and industrial activity (Figure 3). The southwest corner of the SLV primarily consists of residential communities and has the lowest emissions relative to the rest of the valley (Figure 4a).

While the highest CO_2 enhancements in downtown SLC can be partially explained by the juxtaposition of transportation, commercial, and industrial activity, the TRAX Red Line also runs through the middle of heavily trafficked roads surrounded by multi-story buildings in this part of the valley. It is suspected that the exceptionally high CO_2 concentrations measured across downtown SLC are being enhanced by undiluted vehicle tail pipe emissions (Mallia et al., 2020; Mitchell, Lin, et al., 2018). Such effects are not accounted for within mesoscale atmospheric models (Mallia et al., 2020). Therefore, TRAX Red and Green line measurements in downtown SLC were excluded from the inverse analysis. The observations not included in the inverse analysis are grayed out in Figure 2a.

The first step of the 2019 analysis was to compare simulated and observed CO_2 concentrations at the measurement sites located throughout the SLV (UUCON + TRAX) during the afternoon. For this comparison, model-simulated CO_2 concentrations utilized emissions from the prior emission inventory (Figure 3a). The majority of dCO_2 was sourced from emissions within the SLV (>90%). Biospheric contributions of dCO_2 were minimal and only accounted for 8% of the total dCO_2. Afternoon biospheric fluxes from March to April averaged around -0.88 µmol m^{-2} s^{-1}. Limited contributions from biospheric fluxes in the SLV, also found in previous work (Strong et al., 2011), are due to relatively limited biological activity during the early spring. The SLV is also located in a semi-arid environment, with the West Desert being located toward the prevailing wind direction (west).
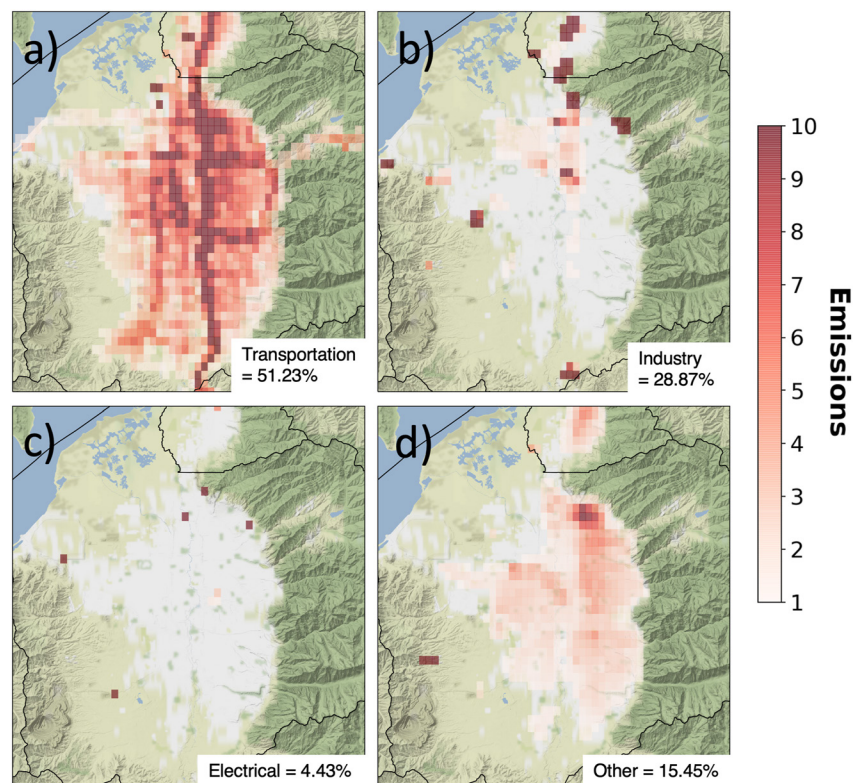
Figure 3. Anthropogenic CO_2 emissions for the Salt Lake Valley (SLV) from the (a) transportation, (b) industrial, (c) electrical power generation, and (d) other sectors. Emissions are in units of μmoles m^{-2} s^{-1}. Each panel also includes the sector contribution of CO_2 for the entire SLV as a percentage. The color scaling is capped at 10 μmol m^{-2} s^{-1}.

Like the observed dCO_2 concentrations along the TRAX Red line, simulated dCO_2 decreased from north to south, with the highest concentrations being co-located with downtown SLC (Figures 2a and 2b). While the highest simulated dCO_2 was in downtown SLC, these values were much smaller relative to the observed enhancements by a factor of 1.6. As described earlier, it is suspected that the observed dCO_2 signal in this part of the valley is partially explained by undiluted tail pipe emissions. Like the observations in Figure 2a, modeled concentrations of dCO_2 were grayed out in Figures 2b and 2c. Modeled dCO_2 remained elevated through the middle of the valley, like the observations (Figures 2a and 2b). Overall, simulated concentrations of CO_2 were about ~3 ppm higher than the observed dCO_2 signal in the middle of the valley (relative bias = +30%). Simulated dCO_2 sharply drops off, like the observations, as the TRAX Red Line veered toward the southwest corner of the SLV. Here, model-observation differences were minimal (<1 ppm, Figures 2a and 2b). On average, TRAX simulated dCO_2 were 1.74 ppm higher than observed enhancements, even when excluding downtown data (Figure 5a). A similar model bias was also observed at many of the UUCON sites (bias = +0.9; Table 1).

All the observations described above, the prior emissions inventory (Figure 4a), model data, including simulated CO_2 concentrations and HYSPLIT-STILT footprints (Figure 4b), were incorporated within a Bayesian inverse analysis. After running the inverse analysis, there was a downward adjustment of afternoon emissions across the SLV (posterior–prior). The largest adjustments were centered across the northern part of the valley, and gradually decreased toward the south (Figures 4c and 4d). The spatial distribution of absolute emission adjustments were likely driven by the large observation-model differences in CO_2, particularly along the northern segment of the TRAX Red line and at the SUG and WBB sites. On average, the afternoon-averaged emissions from the prior were reduced by 26% (159 tC hr^{-1}). 48.65% of the emission adjustments were applied to the transportation sector, while 33.1% of the emission adjustments were allocated to the industrial sector (Table 2). The remaining 18.3% of adjustments were applied to the electrical generation and "other" sectors.

HYSPLIT-STILT simulations of CO_2 were generated using the posterior emissions (Figure 2c). Unsurprisingly, using the posterior emissions reduced modeled dCO_2 across much of the SLV. Previously, modeled dCO_2
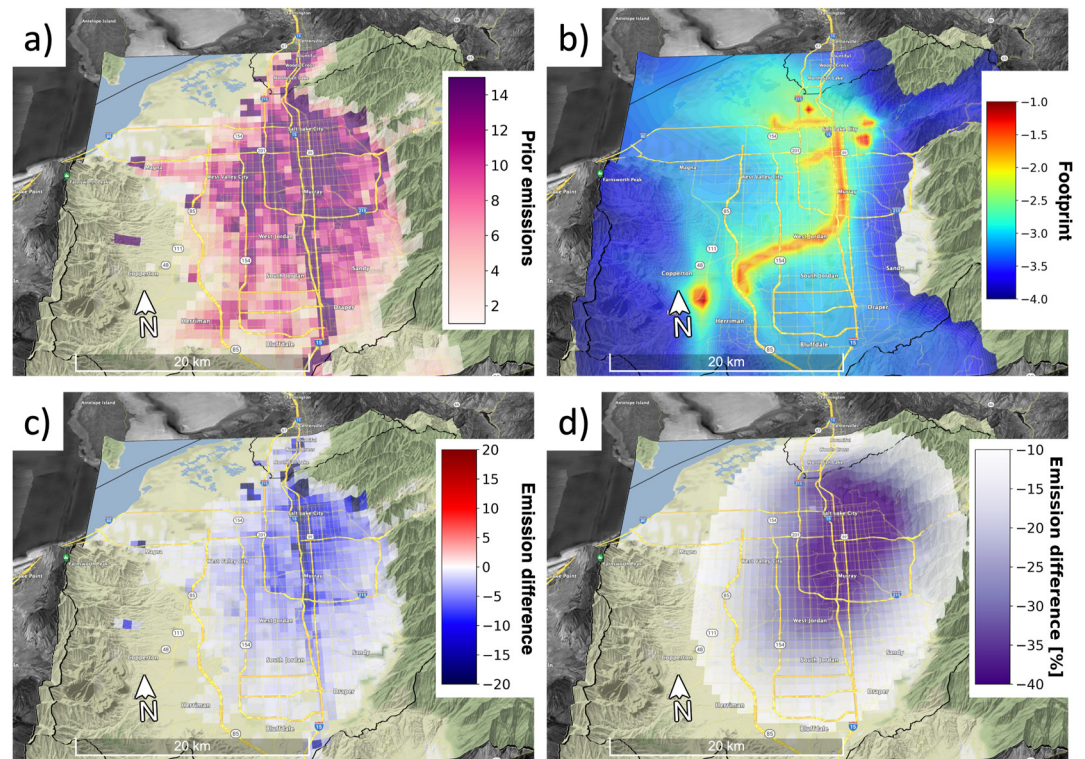
Figure 4. (a) Anthropogenic CO_2 emissions (μmoles m^{-2} s^{-1}) estimated by the prior, (b) HYSPLIT-STILT footprints for all receptors ($\log_{10}$[ppm/μmoles m^{-2} s^{-1}]), excluding receptors along the TRAX lines in downtown SLC, (c) anthropogenic CO_2 emission adjustments after running the inverse analysis, and (d) anthropogenic CO_2 emission adjustments as a percentage for each grid cell. All panels are averaged for the afternoon (1800-0000 UTC) for March through April 2019.

concentrations in the middle of the SLV were overestimated by 30%. After running the inverse analysis, and when using the posterior emissions, modeled biases across this part of the valley were reduced significantly. On average, model-observation mismatches of dCO_2 along the TRAX Red Line were small, with an average bias of -0.28 ppm and a correlation of $r = 0.85$ (Figure 5a). CO_2 simulations at the UUCON sites also observed smaller biases, with most sites reporting smaller or in some cases, negative biases after applying the posterior emission adjustment (Table 1).
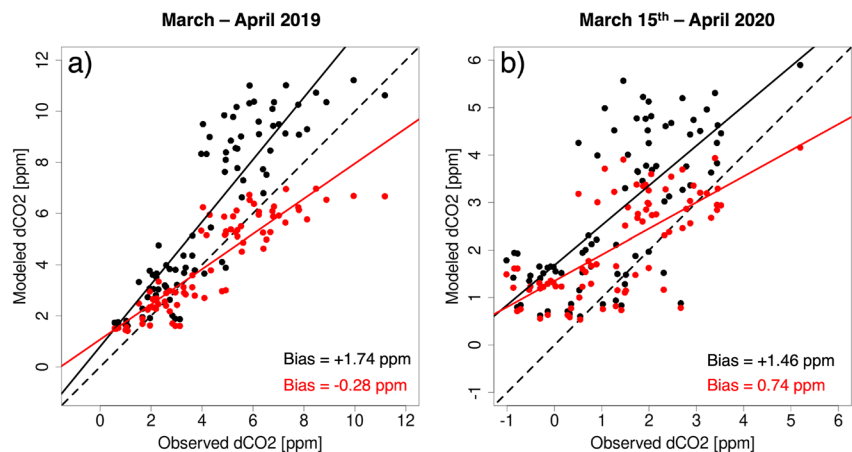

Figure 5. Scatter plots of afternoon-averaged observed and modeled dCO_2 along the TRAX red line for (a) March–April 2019 and (b) March 15th–April 2020. The black (red) circles represent comparisons between the observations and simulated dCO_2 using the prior (posterior) emissions inventory.

Table 1

Modeled dCO_2 Bias (ppm) for All UUCON Sites Using Our Prior and Posterior Emission Estimates for 2019 and 2020

Site	Prior 2019	Posterior 2019	Prior 2020	Posterior 2020
DBK	2.52	1.56	3.46	3.43
IMC	−2.05	−3.19	–	–
RPK	0.23	−1.17	–	–
SUG	3.18	0.67	4.03	3.02
WBB	0.62	−0.65	3.21	2.53
mean	0.90	−0.56	3.57	2.99

Note. Averaging periods only includes the afternoon hours for March and April. The 2020 analysis only includes data starting from the beginning of the lockdown period (March 15th) thought the end of April.

The posterior emission inventory generated as part of this analysis was used as the prior for the 2020 COVID-19 lockdown analysis.

3.2. Inverse Model Results 2020

Between the second week of March through the end of April, traffic activity across Salt Lake County decreased by ∼30% according to the Utah Department of Transportation (UDOT; Figure 6a) due to the COVID-19 lockdown. The lowest traffic levels were detected during the first week of April (−38%) and gradually rebounded through the end of April. Unfortunately, there was limited activity data available that described changes in other emission sectors such as the industrial and electricity production sectors.

Like 2019, CO_2 concentrations along the TRAX Red Line exhibited significant spatial variability. dCO_2 were highest near downtown SLC, and decreased across the middle of the valley, before dropping to near-background levels in the southwest corner of the valley (Figure 6b). Relative to 2019, dCO_2 along the TRAX Red Line was lower by 2 ppm. Differences in dCO_2 for 2020 versus 2019 were greatest near downtown SLC (−5 ppm). Differences between 2019 and 2020 were lower in the middle part of the SLV (−1 to 2 ppm), and nearly indistinguishable across the southwest corner of the valley. This result can be explained by downtown SLC's concentration of commercial activity, which likely observed a notable shift of the commuting workforce to furlough or remote work during the COVID-19 lockdown. A similar difference was also observed along the TRAX Green Line when comparing 2019 and 2020 (Figure 6c). Like the TRAX Red Line, CO_2 measurements along the Green Line were lower by ∼3 ppm, with differences as large as 5 ppm near downtown SLC.

Two of the sites (RPK & IMC) were unavailable during the spring. However, HDP, SUG, WBB, and DBK sites were operational during the COVID-19 lockdown. There were also a limited number of TRAX transects during the final week of March. Nonetheless, the TRAX car was in operation during other times in March and throughout all of April, and made 118 transects along the Red Line, and 29 along the Green Line. From March 15th to April 30th, TRAX measurements were available on 22 of 45 possible days during the afternoon.

Prior to running our inversion, model-simulated dCO_2 was overestimated across much of the SLV (Figures 7a and 7b). These simulations used the posterior emissions estimated from the 2019 inverse analysis (Figure 8a). Like 2019, biospheric flux contributions were small, and accounted for less than 10% of the total dCO_2 signal. Afternoon-averaged CO_2 uptake from the biosphere was 25% less relative to 2019 (−0.68 μmol m^{-2} s^{-1}). On average, simulated dCO_2 along the TRAX Red Line were overpredicted by 1.46 ppm when excluding downtown data (Figures 7a and 7b). dCO_2 concentrations were overpredicted by ∼2 ppm across the middle of the SLV, while the southwest corner of the SLV observed smaller overestimates (∼1 ppm). dCO_2 was also overpredicted at the UUCON sites during the COVID-19 lockdown period, with biases ranging between +3.2 and +4 ppm (Table 1).

Results from the COVID-19 lockdown inversion indicated a 20% (90.5 tC hr^{-1}) reduction in emissions across the SLV between March 15th through April 30th (Figures 8c and 8d) during the afternoon. Prior to running the inverse analysis for 2020, the SLV study domain emitted 453.1 tC hr^{-1} on average, while the inverse analysis reduced afternoon-average emissions to 362.4 tC hr^{-1}. The largest reductions were confined to the northern part of the SLV, with emission reductions gradually decreasing to the southwest (Figure 8c). The largest emission

Table 2

Emission Changes Partitioned by Sector for 2019 and 2020 Inversions

Sector	2019	2020 (6-km)	2020 (3-km)	2020 (9-km)	2020 (1-day)	2022 (3-day)
Electrical	2.8%	3.3%	3.2%	3.6%	3.3%	3.3%
Industrial	33.1%	38.2%	42.0%	36.5%	38.2%	38.5%
Transportation	48.7%	44.0%	41.0%	45.2%	44.0%	43.8%
Other	15.5%	14.5%	13.9%	14.8%	14.5%	14.5%

Note. The last four columns also represent the inverse analysis carried out for 2020 but using a spatial correlation length scale of 3 and 9-km, and temporal correlation timescale of 1 and 3 days.
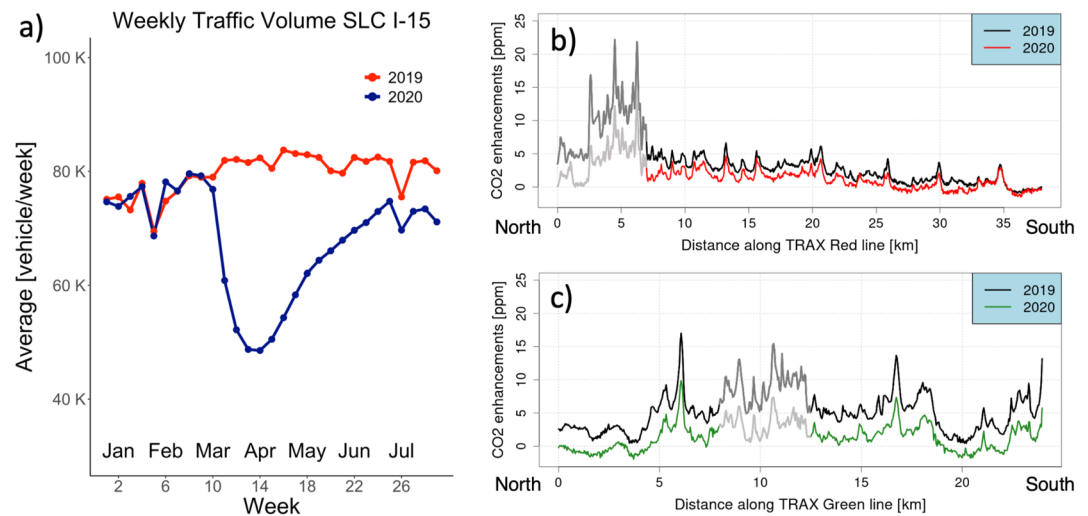
Figure 6. (a) Average vehicles per week along I-15 for the first 6 months of 2019 and 2020 from UDOT. Afternoon-averaged dCO_2 (1800-0000 UTC) for March 15th–30 April 2019 and 2020 along the (b) TRAX Red and (c) Green lines. The distance along the TRAX lines (x axis) starts in the northern-most location of each train line. The gray shaded lines in panel (b and c) denotes sections of the TRAX Red and Green lines that run through downtown SLC, which were not included in the inverse analysis.

reductions were associated with major industrial point sources across the northern part of the valley, the Salt Lake International Airport, and along major roadways such as I-15, 80, and 215. For the 2020 inverse analysis, 38.2% (34.4 tC hr^{-1}) of the emission reductions were applied to the industrial sector, while 43.95% (39.8 tC hr^{-1}) of the emission reductions were allocated to the transportation sector (Table 2). ∼18% (16.3 tC hr^{-1}) of the remaining
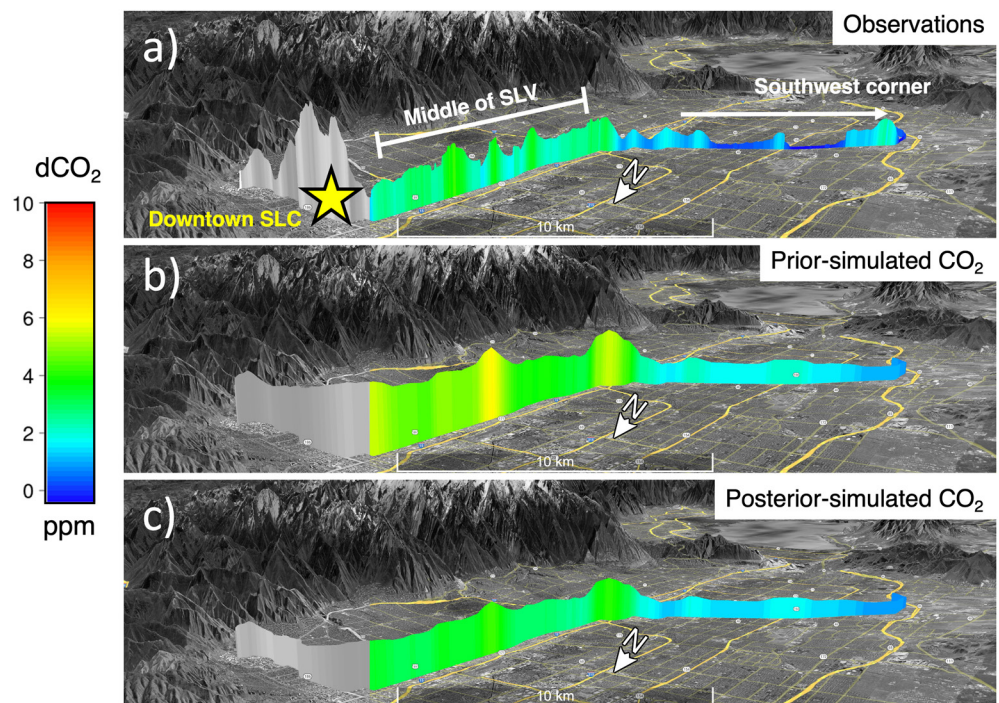

Figure 7. Afternoon-averaged dCO_2 along the TRAX Red line for March 15th though April 2020. (a) Observed and model-simulated dCO_2 using the (b) prior and (c) posterior emissions. The color and height of the colored lines is proportional to the magnitude of dCO_2. The gray shaded lines for dCO_2 correspond to downtown SLC. dCO_2 concentrations in downtown SLC were not included as part of the inverse analysis.
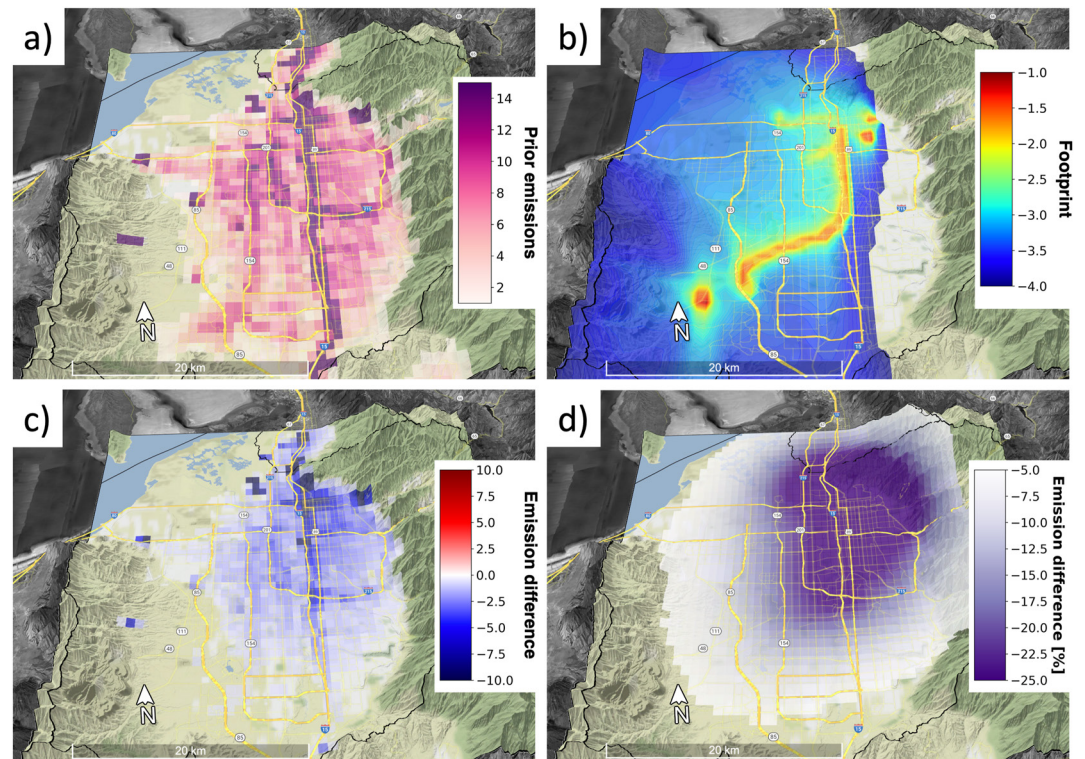
Figure 8. (a) Anthropogenic CO_2 emissions (μmoles m^{-2} s^{-1}) estimated by the prior, (b) HYSPLIT-STILT footprints for all receptors ($\log_{10}$[ppm/μmoles m^{-2} s^{-1}]), excluding receptors along the TRAX lines in downtown SLC, (c) anthropogenic CO_2 emission adjustments after running the inverse analysis (μmoles m^{-2} s^{-1}), and (d) anthropogenic CO_2 emission adjustments as a percentage for each grid cell. All panels are averaged for the afternoon (1800-0000 UTC) for March 15th through April 2020.

emission reductions were from the electrical generation and "other" sectors (Table 2). The sector adjustment percentages between the 2019 and 2020 were similar (Table 2), even though the adjustments in emissions for each year were being driven by different mechanisms (changes in 2020 are presumably caused by the COVID-19 lockdown). For both 2019 and 2020, the emission reductions were primarily centered across the northern part of the SLV (Figures 4c and 8c). It is hypothesized that the similarity between 2019 and 2020 is a result of the northern part of the SLV (a) being co-located with the highest emissions, (b) an area where model-observation mismatches are the largest, and (c) having better sampling relative to other areas in the SLV. It is also worth emphasizing that the emission reductions applied to the transportation sector could be underestimated, while reductions applied to other sectors could be overestimated. During the COVID-19 lockdown, UDOT-estimated traffic activity saw an average decrease of ~30% between March 15th and April 30th. The transportation sector makes up 51% of the emissions across the SLV. Using the UDOT traffic information as a proxy, a ~15% reduction in overall emissions due to traffic would be expected, which would represent ~75% of the modeled 20% emission reduction. According to the inverse analysis, the fraction of the total adjustment attributed to transportation was ~44%. Regardless, both analyses indicate that sectors unrelated to transportation likely had non-negligible reductions in CO_2 emissions during the first COVID-19 lockdown.

Model simulations of CO_2 were generated using the posterior emissions created from the inverse model analysis. Overall, simulated dCO_2 concentrations were improved across much of the SLV (Figure 7c). Prior to running the inverse model analysis, dCO_2 was overpredicted by 1.46 ppm along the TRAX Red Line (Figure 5b). After running the inverse analysis, this overestimate was reduced by ~50% (bias = +0.74 ppm; Figure 5b). The TRAX Green Line (not shown) also observed a ~50% improvement in modeled biases. Some of the modeled overpredictions were eliminated for the UUCON sites (Table 1), albeit an overprediction of ~3 ppm was still present.

A series of sensitivity analyses were carried out to determine how the spatiotemporal correlation parameters l_x and l_t, which were used to construct the prior covariance matrix, would impact emission adjustments. Overall,
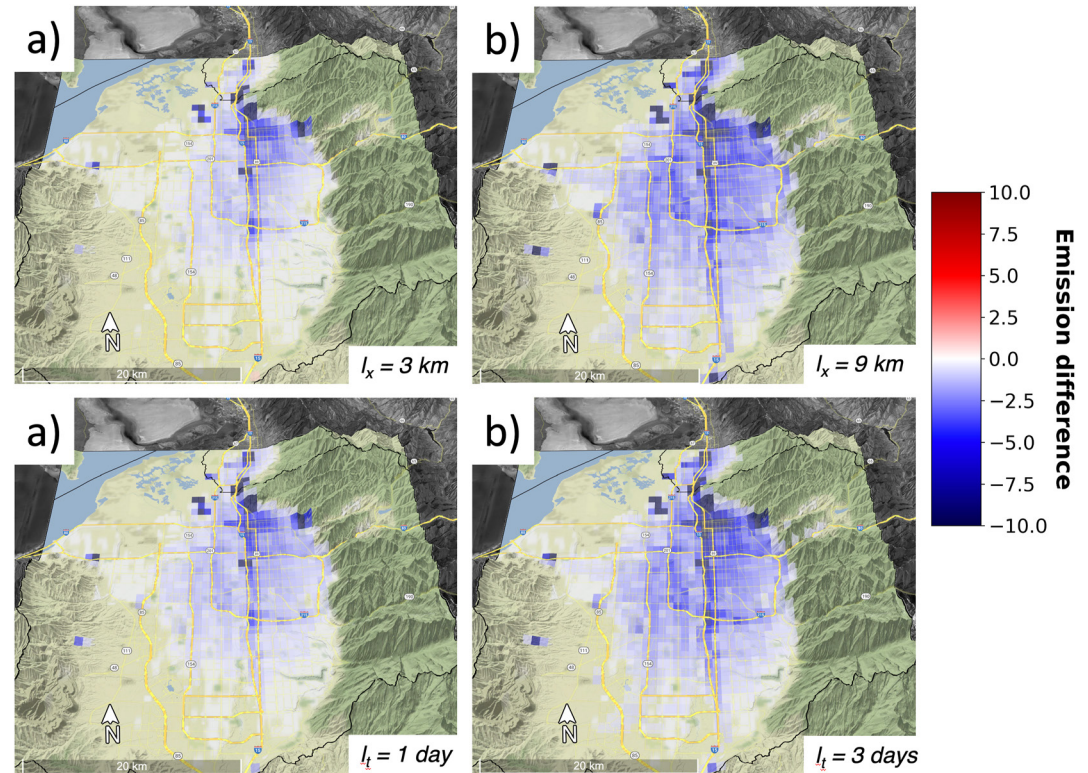
Figure 9. Anthropogenic CO_2 emission adjustments (μmoles m^{-2} s^{-1}) after running an inverse analysis using a spatial length scale of (a) 3 and (b) 9-km and a temporal length scale of (c) 1 and (d) 3 days. All panels are averaged for the afternoon (1800-0000 UTC) for March 15th through April 2020.

varying l_x between 3 and 9-km, and l_t between 1 and 3 days, resulted in emission reductions that ranged between 11% (44.9 tC hr^{-1}) and 24% (108.8 tC hr^{-1}) (Figure 9). Emission reduction partitioning between each sector remained relatively unchanged between the different model configurations (Table 2). These results suggest that there is some underlying uncertainty in the inverse analysis given that the "true" spatiotemporal correlation value is unknown and is difficult to measure. A more detailed description this analysis can be found in the Supporting Information S1 (Text S4).

4. Summary

A Bayesian Inverse analysis was carried out to determine how the COVID-19 lockdown impacted CO_2 emissions across the SLV. This study leveraged two different CO_2 monitoring networks, which included a stationary CO_2 monitoring network and mobile measurements of CO_2 collected on the top of a light rail train that was running semi-continuously during the COVID-19 lockdown. While several studies have already explored how the COVID-19 lockdown impacted urban GHG emissions, there has been limited work determining whether changes in CO_2 for medium-sized cities like SLC are detectable. Furthermore, the COVID-19 lockdown measures were less stringent in SLC (Hallas et al., 2021), which would have presumably lowered CO_2 emission reductions in SLC relative to other cities. Cities, such as Paris and San Francisco observed much larger reductions in CO_2 emissions that ranged between 30% and 50% (Lian et al., 2022; Nalini et al., 2022; Turner et al., 2020; Yadav et al., 2021), where it would be easier to detect emission changes with a CO_2 monitoring network. Finally, there has been limited work on determining whether alternative CO_2 measurement strategies, such as mobile observations, can detect urban-scale emission changes.

Large uncertainties often exist within emission inventories, especially at the urban scale. One unique aspect of this work is that prior to running an inverse analysis for the COVID-19 lockdown, emissions were constrained for 2019 to remove inherent biases within the prior emission inventory. These emissions were then used as the prior emissions for the COVID-19 lockdown analysis. Here it is assumed that emission changes between 2019

and 2020, in the absence of COVID-19, would have been small. An inverse model analysis was then carried out for the COVID-19 lockdown period between March 15 to 30 April 2020. Overall, average emissions across the SLV were adjusted downward by ∼20% during the afternoon (90.5 tC hr^{-1}). The largest emission reductions were confined to the northern part of the SLV, near downtown SLC, where emission reductions were as large as 50%. Downtown SLC is co-located with significant commercial activity with commuting workers, which would have been most impacted by the COVID-19 lockdown. It is worth noting that the COVID-19 emission reductions estimated in SLC are lower than other cities such as Los Angeles, Paris, the Bay Area (Lian et al., 2022; Nalini et al., 2022; Turner et al., 2020; Yadav et al., 2021). It is suspected that less stringent lockdown measures in SLC relative to other cities across the U.S were the driving factors behind the smaller emission reductions.

The largest fraction of afternoon emission reductions were applied to the transportation (43.95%; 39.8 tC hr^{-1}) and industrial sectors (38%; 34.4 tC hr^{-1}). It is also worth emphasizing that it is difficult to quantify sector-level emission reductions, even with semi-continuous mobile measurements like TRAX. For example, it is suspected that the fraction of emission reductions from the transportation sector could reach 75% (67.9 tC hr^{-1}) based on traffic activity data collected by UDOT. However, it is difficult to ascertain specific reductions by sector without activity data for other emission sectors. For example, industrial activity data was not available during this analysis. Emission adjustments were also highly sensitive to the spatiotemporal correlation length scale parameter with emission reductions ranging between 11% and 25% (44.9 tC hr^{-1} to 108.8 tC hr^{-1}) depending on the length scale select.

While CO_2 monitoring methods can track large-scale decarbonization as suggested by the analysis carried out here and in other studies, linking emission changes to specific emission sectors remain challenging. Activity data at a high temporal resolution for industrial sources, which can account for a large fraction of urban CO_2 emissions, is challenging to obtain. Therefore, CO_2 monitoring networks that specifically target industrial emission sources are sorely needed. Research is also needed to quantify to what extent can carbon monitoring networks track decarbonization efforts. Decarbonization will likely occur gradually; therefore, it will be necessary to determine the "limit of detection" of current CO_2 monitoring strategies.

Ultimately, the analysis carried out here suggests that inverse models, combined with stationary and mobile CO_2 observations, can track modest emission reductions in medium-sized cities, and to some degree, geographically identify emission reductions at the city-scale. In situ urban CO_2 observation networks and new satellite-based measurements approaches will likely play a pivotal role toward monitoring decarbonization efforts in cities across the globe.

Data Availability Statement

Biospheric fluxes for northern Utah were estimated using the SMUrF data set, which is publicly available at the Oak Ridge National Lab data base (Wu, 2021). Anthropogenic emissions for the northern Utah were obtained from the Vulcan emission inventory, which is downloadable from the Oak Ridge National Lab database (Gurney et al., 2019). The HYSPLIT-STILT v5.0.0 software was used to generate the spatiotemporal influence matrix for each measurement (NOAA ARL, 2020). Meteorological data used to drive HYSPLIT-STILT backward trajectories were generated by output from the Weather Research and Forecast model v4.2 software available at NCAR: https://www2.mmm.ucar.edu/wrf/users/download/get_source.html (Skamarock et al., 2019). Utah traffic data for 2019 and 2020 is publicly available on the Utah Department of Transportation's webpage (UDOT, 2023). TRAX and UUCON CO_2 data is hosted by the University of Utah and is publicly available at https://air.utah.edu (Lin et al., 2018).

References

Bares, R., Mitchell, L., Fasoli, B., Bowling, D. R., Catharine, D., Garcia, M., et al. (2019). The Utah urban carbon dioxide (UUCON) and Uintah basin greenhouse gas networks: Instrumentation, data, and measurement uncertainty. *Earth System Science Data*, 11(3), 1291–1308. https://doi.org/10.5194/essd-11-1291-2019

Bréon, F. M., Broquet, G., Puygrenier, V., Chevallier, F., Xueref-Remy, I., Ramonet, M., et al. (2015). An attempt at estimating Paris area CO_2 emissions from atmospheric concentration measurements. *Atmospheric Chemistry and Physics*, 15(4), 1707–1724. https://doi.org/10.5194/acp-15-1707-2015

Ciais, P., Dolman, A. J., Bombelli, A., Duran, R., Peregon, A., Rayner, P. J., et al. (2014). Current systematic carbon-cycle observations and the need for implementing a policy-relevant carbon observing system. *Biogeosciences*, 11(13), 3547–3602. https://doi.org/10.5194/bg-11-3547-2014

Enting, I. G. (2002). *Inverse problems in atmospheric constituent transport*. Cambridge University Press.

Fasoli, B., Lin, J. C., Bowling, D. R., Mitchell, L., & Mendoza, D. (2018). Simulating atmospheric tracer concentrations for spatially distributed receptors: Updates to the stochastic time-inverted Lagrangian transport model's R interface (STILT-R version 2). *Geoscientific Model Development*, *11*(7), 2813–2824. https://doi.org/10.5194/gmd-11-2813-2018

Gately, C. K., & Hutyra, L. R. (2017). Large uncertainties in urban-scale carbon emissions. *Journal of Geophysical Research: Atmospheres*, *122*(20), 11142–11260. https://doi.org/10.1002/2017jd027359

Gensheimer, J., Turner, A. J., Shekhar, A., Wenzel, A., Keutsch, F. N., & Chen, J. (2021). What are the different measures of mobility telling us about surface transportation CO2 emissions during the COVID-19 pandemic? *Journal of Geophysical Research: Atmospheres*, *126*(11), e2021JD034664. https://doi.org/10.1029/2021jd034664

Gerbig, C., Körner, S., & Lin, J. C. (2008). Vertical mixing in atmospheric tracer transport models: Error characterization and propagation. *Atmospheric Chemistry and Physics*, *8*(3), 591–602. https://doi.org/10.5194/acp-8-591-2008

Gurney, K. R., Liang, J., Patarasuk, R., Song, Y., Huang, J., & Roest, G. (2019). Vulcan: High-Resolution annual fossil fuel CO_2 emissions in USA, 2010-2015. (Version 3) [Dataset]. ORNL DAAC. https://daac.ornl.gov/NACP/guides/Vulcan_V3_Annual_Emissions.html

Gurney, K. R., Liang, J., Patarasuk, R., Song, Y., Huang, J., & Roest, G. (2020). The Vulcan version 3.0 high-resolution fossil fuel CO_2 emissions for the United States. *Journal of Geophysical Research: Atmospheres*, *125*(19), e2020JD032974. https://doi.org/10.1029/2020jd032974

Gurney, K. R., Liang, J., Roest, G., Song, Y., Mueller, K., & Lauvaux, T. (2021). Under-reporting of greenhouse gas emissions in US cities. *Nature Communications*, *12*(1), 1–7. https://doi.org/10.1038/s41467-020-20871-0

Gurney, K. R., Romero-Lankao, P., Seto, K. C., Hutyra, L. R., Duren, R. M., Kennedy, C., et al. (2015). Track urban emissions on a human scale. *Nature*, *525*(7568), 179–181. https://doi.org/10.1038/525179a

Hallas, L., Hatibie, A., Koch, R., Majumdar, S., Pyarali, M., Wood, A., & Hale, T. (2021). Variation in US states' responses to COVID-19 3.0. Retrieved from https://www.bsg.ox.ac.uk/research/publications/variation-us-states-responses-covid-19

Hsu, A., Höhne, N., Kuramochi, T., Roelfsema, M., Weinfurter, A., Xie, Y., et al. (2019). A research roadmap for quantifying non-state and subnational climate mitigation action. *Nature Climate Change*, *9*(1), 11–17. https://doi.org/10.1038/s41558-018-0338-z

IPCC. (2013). Climate change 2013: The physical science basis. Contribution of working group I to the fifth assessment report of the intergovernmental panel on climate change.

IPCC. (2018). Global Warming of 1.5°C. An IPCC Special Report on the impacts of global warming of 1.5°C above pre-industrial levels and related global greenhouse gas emission pathways. In *The context of strengthening the global response to the threat of climate change, sustainable development, and efforts to eradicate poverty*.

Kunik, L., Mallia, D. V., Gurney, K. R., Mendoza, D. L., Oda, T., & Lin, J. C. (2019). Bayesian inverse estimation of urban CO_2 emissions: Results from a synthetic-data simulation over Salt Lake City, UT. *Elementa*, *7*(1), 36. https://doi.org/10.1525/elementa.375

Lauvaux, T., Miles, N. L., Deng, A., Richardson, S. J., Cambaliza, M. O., Davis, K. J., et al. (2016). High-resolution atmospheric inversion of urban CO_2 emissions during the dormant season of the Indianapolis Flux Experiment (INFLUX). *Journal of Geophysical Research: Atmospheres*, *121*(10), 5213–5236. https://doi.org/10.1002/2015jd024473

Le Quéré, C., Peters, G. P., Friedlingstein, P., Andrew, R. M., Canadell, J. G., Davis, S. J., et al. (2021). Fossil CO_2 emissions in the post-COVID-19 era. *Nature Climate Change*, *11*(3), 197–199. https://doi.org/10.1038/s41558-021-01001-0

Lian, J., Bréon, F. M., Broquet, G., Lauvaux, T., Zheng, B., Ramonet, M., et al. (2022). Sensitivity to the sources of uncertainties in the modeling of atmospheric CO_2 concentration within and in the vicinity of Paris. *Atmospheric Chemistry and Physics*, *21*(13), 10707–10726. https://doi.org/10.5194/acp-21-10707-2021

Lin, J. C., Gerbig, C., Wofsy, S. C., Andrews, A. E., Daube, B. C., Davis, K. J., & Grainger, C. A. (2003). A near-field tool for simulating the upstream influence of atmospheric observations: The Stochastic Time-Inverted Lagrangian Transport (STILT) model. *Journal of Geophysical Research*, *108*(D16), 4493.

Lin, J. C., Mitchell, L., Crosman, E., Mendoza, D. L., Buchert, M., Bares, R., et al. (2018). CO_2 and carbon emissions from cities: Linkages to air quality, socioeconomic activity, and stakeholders in the Salt Lake City urban area. *Bull. Am. Meteor. Soc.*, *99*(11), 2325–2339. https://doi.org/10.1175/bams-d-17-0037.1

Loughner, C., Fasoli, B., Stein, A. F., & Lin, J. C. (2021). Incorporating features from the stochastic time-inverted Lagrangian transport (STILT) model into the hybrid single-particle Lagrangian integrated trajectory (HYSPLIT) model: A unified dispersion model for time-forward and time-reversed applications. *Journal of Applied Meteorology and Climatology*, *60*, 799–810. https://doi.org/10.1175/jamc-d-20-0158.1

Mallia, D. V., Kochanski, A., Pennell, C., Oswald, W., & Lin, J. C. (2017). Wind-blown dust modeling using a backward Lagrangian particle dispersion model. *Journal of Applied Meteorology and Climatology*, *56*(10), 2845–2867. https://doi.org/10.1175/jamc-d-16-0351.1

Mallia, D. V., Lin, J. C., Urbanski, S., Ehleringer, J., & Nehrkorn, T. (2015). Impacts of upwind wildfire emissions on CO, CO_2, and $PM_{2.5}$ concentrations in Salt Lake City, Utah. *Journal of Geophysical Research: Atmospheres*, *120*(1), 147–166. https://doi.org/10.1002/2014jd022472

Mallia, D. V., Mitchell, L. E., Kunik, L., Fasoli, B., Bares, R., Gurney, K. R., et al. (2020). Constraining urban CO_2 emissions using mobile observations from a light rail public transit platform. *Environmental Science & Technology*, *54*(24), 15613–15621. https://doi.org/10.1021/acs.est.0c04388

McKain, K., Wofsy, S. C., Nehrkorn, T., Eluszkiewicz, J., Ehleringer, J. R., & Stephens, B. B. (2012). Assessment of ground-based atmospheric observations for verification of greenhouse gas emissions from an urban region. *Proceedings of the National Academy of Sciences of the United States of America*, *109*(22), 8423–8428. https://doi.org/10.1073/pnas.1116645109

Mitchell, L. E., Crosman, E. T., Jacques, A. A., Fasoli, B., Leclair-Marzolf, L., John Horel, L., et al. (2018). Monitoring of greenhouse gases and pollutants across an urban area using a light-rail public transit platform. *Atmospheric Environment*, *187*, 9–23. https://doi.org/10.1016/j.atmosenv.2018.05.044

Mitchell, L. E., Lin, J. C., Bowling, D. R., Pataki, D. E., Strong, C., Schauer, A. J., et al. (2018). Long-term urban carbon dioxide observations reveal spatial and temporal dynamics related to urban characteristics and growth. *Proceedings of the National Academy of Sciences of the United States of America*, *115*(12), 2912–2917. https://doi.org/10.1073/pnas.1702393115

Nalini, K., Lauvaux, T., Abdallah, C., Lian, J., Ciais, P., Utard, H., et al. (2022). High-resolution Lagrangian inverse modeling of CO_2 emissions over the Paris region during the first 2020 lockdown period. *Journal of Geophysical Research: Atmospheres*, *127*(14), e2021JD036032. https://doi.org/10.1029/2021jd036032

Nehrkorn, T., Eluszkiewicz, J., Wofsy, S. C., Lin, J. C., Gerbig, C., Longo, M., & Freitas, S. (2010). Coupled weather research and forecasting–stochastic time-inverted Lagrangian transport (WRF–STILT) model. *Meteorology and Atmospheric Physics*, *107*(1–2), 51–64. https://doi.org/10.1007/s00703-010-0068-x

Nickless, A., Rayner, P. J., Engelbrecht, F., Brunke, E. G., Erni, B., & Scholes, R. J. (2018). Estimates of CO_2 fluxes over the city of Cape Town, south Africa, through Bayesian inverse modelling. *Atmospheric Chemistry and Physics*, *18*(7), 4765–4801. https://doi.org/10.5194/acp-18-4765-2018

Nisbet, E., & Weiss, R. (2010). Top-down versus bottom-up. *Science*, *328*(5983), 1241–1243. https://doi.org/10.1126/science.1189936

NOAA ARL (2020). HYSPLIT model. (Version 5.0.0) [Software]. NOAA ARL. https://www.arl.noaa.gov/hysplit

Oda, T., Lauvaux, T., Lu, D., Rao, P., Miles, N. L., Richardson, S. J., & Gurney, K. R. (2017). On the impact of granularity of space-based urban CO_2 emissions in urban atmospheric inversions: A case study for Indianapolis. *Elementa: Science of the Anthropocene*, *5*. https://doi.org/10.1525/elementa.146

Oda, T., Maksyutov, S., & Andres, R. J. (2018). The open-source data inventory for anthropogenic CO_2, version 2016 (ODIAC2016): A global monthly fossil fuel CO_2 gridded emissions data product for tracer transport simulations and surface flux inversions. *Earth System Science Data*, *10*(1), 87–107. https://doi.org/10.5194/essd-10-87-2018

Pataki, D. E., Bowling, D. R., & Ehleringer, J. R. (2003). Seasonal cycle of carbon dioxide and its isotopic composition in an urban atmosphere: Anthropogenic and biogenic effects. *Journal of Geophysical Research*, *108*(4735), 4735. https://doi.org/10.1029/2003jd003865

Pitt, J. R., Lopez-Coto, I., Hajny, K. D., Tomlin, J., Kaeser, R., Jayarathne, T., et al. (2022). New York City greenhouse gas emissions estimated with inverse modeling of aircraft measurements. *Elementa: Science of the Anthropocene*, *10*, 1. https://doi.org/10.1525/elementa.2021.00082

Roest, G. S., Gurney, K. R., Miller, S. M., & Liang, J. (2020). Informing urban climate planning with high resolution data: The Hestia fossil fuel CO_2 emissions for Baltimore, Maryland. *Carbon Balance and Management*, *15*(1), 1–16. https://doi.org/10.1186/s13021-020-00157-0

Skamarock, W. C., Klemp, J. B., Dudhia, J., Gill, D. O., Liu, Z., & Berner, J. (2019). *A description of the advanced research WRF Version 4. NCAR Tech. Note* (p. 145). NCAR/TN-556+STR.

Staufer, J., Broquet, G., Bréon, F. M., Puygrenier, V., Chevallier, F., Xueref-Rémy, I., et al. (2016). The first 1-year-long estimate of the Paris region fossil fuel CO_2 emissions based on atmospheric inversion. *Atmospheric Chemistry and Physics*, *16*(22), 14703–14726. https://doi.org/10.5194/acp-16-14703-2016

Stephens, B. B., Miles, N. L., Richardson, S. J., Watt, A. S., & Davis, K. J. (2011). Atmospheric CO_2 monitoring with single-cell NDIR-based analyzers. *Atmospheric Measurement Techniques*, *4*(12), 2737–2748. https://doi.org/10.5194/amt-4-2737-2011

Strong, C., Stwertka, C., Bowling, D. R., Stephens, B. B., & Ehleringer, J. R. (2011). Urban carbon dioxide cycles within the Salt Lake Valley: A multiple-box model validated by observations. *Journal of Geophysical Research*, *116*(D15), D15307. https://doi.org/10.1029/2011jd015693

Tarantola, A. (1987). *Inverse problem theory methods for data fitting and model parameter estimation*. Elsevier Science B.V.

Turner, A. J., Kim, J., Fitzmaurice, H., Newman, C., Worthington, K., Chan, K., et. al. (2020). Observed impacts of COVID-19 on urban CO_2 emissions. *Geophysical Research Letters*, *47*(22), e2020GL090037. https://doi.org/10.1029/2020gl090037

UDOT. (2023). Traffic operations data [Dataset]. UDOT. Retrieved from https://www.udot.utah.gov/connect/business/traffic-data/traffic-operations-data/

Wu, D. (2021). Urban biogenic CO_2 fluxes: GPP, Reco and NEE estimates from SMUrF, 2010-2019 (version 1). [Dataset]. ORNL DAAC. https://www.arl.noaa.gov/hysplit

Wu, D., Lin, J. C., Duarte, H. F., Yadav, V., Parazoo, N. C., Oda, T., & Kort, E. A. (2021). A model for urban biogenic CO_2 fluxes: Solar-induced fluorescence for modeling Urban biogenic Fluxes (SMUrF v1). *Geoscientific Model Development*, *14*(6), 3633–3661. https://doi.org/10.5194/gmd-14-3633-2021

Yadav, V., Ghosh, S., Mueller, K., Karion, A., Roest, G., Gourdji, S. M., et al. (2021). The impact of COVID-19 on CO_2 emissions in the Los Angeles and Washington DC/Baltimore metropolitan areas. *Geophysical Research Letters*, *48*(11), e2021GL092744. https://doi.org/10.1029/2021gl092744